*photonics*

MDPI

*Review*

# Fluorometric Mercury (II) Detection Using Heteroatom-Doped Carbon and Graphene Quantum Dots

**Mosayeb Chaghazardi [1], Soheila Kashanian [1,2,*], Maryam Nazari [1], Kobra Omidfar [3,4], Yvonne Joseph [5,6] and Parvaneh Rahimi [5,6,*]**

[1] Faculty of Chemistry, Razi University, Kermanshah 67149, Iran; m.chaghazardi@razi.ac.ir (M.C.); nazari.maryam@razi.ac.ir (M.N.)
[2] Department of Nanobiotechnology, Faculty of Innovative Science and Technology, Razi University, Kermanshah 67149, Iran
[3] Biosensor Research Center, Endocrinology and Metabolism Molecular—Cellular Sciences Institute, Tehran University of Medical Sciences, Tehran 1416753955, Iran; omidfar@tums.ac.ir
[4] Endocrinology and Metabolism Research Center, Endocrinology and Metabolism Clinical Sciences Institute, Tehran University of Medical Sciences, Tehran 1416753955, Iran
[5] Institute of Nanoscale and Biobased Materials, Faculty of Materials Science and Technology, Technische Universität Bergakademie Freiberg, 09599 Freiberg, Germany; yvonne.joseph@esm.tu-freiberg.de
[6] Freiberg Center for Water Research, Technische Universität Bergakademie Freiberg, 09599 Freiberg, Germany
* Correspondence: kashanian_s@yahoo.com (S.K.); parvaneh.rahimi@esm.tu-freiberg.de (P.R.)

**Abstract:** Mercury ion ($Hg^{2+}$) is one of the most toxic pollutants that can exist throughout the environment and be diffused into water, soil, air, and eventually the food chain. Even a very low level of $Hg^{2+}$ diffused in living organisms can hurt their DNA and cause the permanent damage of the central nervous system and a variety of consequential disorders. Hence, the development of a sensitive and specific method for the detection of $Hg^{2+}$ at trace ranges is extremely important as well as challenging. Fluorometric detection assays based on graphene quantum dots (GQDs) and carbon quantum dots (CQDs) offer considerable potential for the determination and monitoring of heavy metals due to their fascinating properties. Although the quantum yield of GQDs and CQDs is sufficient for their use as fluorescent probes, doping with heteroatoms can significantly improve their optical properties and selectivity toward specific analytes. This review explores the primary advances of CQDs and GQDs in their great electronic, optical, and physical properties, their synthetic methods, and their use in $Hg^{2+}$ fluorimetry detection.

**Keywords:** mercury; carbon quantum dots; graphene quantum dots; fluorescent sensors



**Citation:** Chaghazardi, M.; Kashanian, S.; Nazari, M.; Omidfar, K.; Joseph, Y.; Rahimi, P. Fluorometric Mercury (II) Detection Using Heteroatom-Doped Carbon and Graphene Quantum Dots. *Photonics* **2024**, *11*, 841. https://doi.org/10.3390/photonics11090841

Received: 16 August 2024
Revised: 29 August 2024
Accepted: 3 September 2024
Published: 5 September 2024



## 1. Introduction

Mercury ion ($Hg^{2+}$) is known as one of the most toxic heavy metals, with features such as bioaccumulation and strong toxicity. It has been proven that $Hg^{2+}$ can simply diffuse through the tissues and skin, thereby impairing central mitosis, DNA, and the nervous system. So even at very low concentrations, it can cause the permanent damage of the central nervous system and critical problems for human health [1]. Actually, mercury toxicity is attributed to cellular dysfunction in organisms because of its strong affinity and conjugation with the thiol groups (-SH) and seleno groups (-SeH) of enzymes and proteins [2]. Thus, the major building blocks of enzymes and proteins are made due to forming strong mercury complexes with amino acids, and serious neurotoxicity and hepatotoxicity occur [3]. For example, $Hg^{2+}$ can be converted by bacteria in aquatic sediments into methylmercury, a highly toxic form of mercury, and can consequently accumulate in the human body through the food chain, causing many brain and neurological diseases by blocking related proteins. According to the United States Environment Protection Agency (EPA) and the World Health Organization (WHO), the maximum permissible concentrations of $Hg^{2+}$ in drinking water are 2.0 and 6.0 μg/L, respectively. Therefore, designing a sensitive, accurate, and

selective analytical technique for $Hg^{2+}$ sensing in water samples is highly important and challenging for water quality considerations. There are numerous analytical procedures for the mercury recognition in practice, including auger-electron spectroscopy [4], inductively coupled plasma-mass spectrometry (ICP-MS) [5,6], cold-vapor atomic absorption spectrometry (CV-AAS) [7,8], cold-vapor atomic fluorescence spectroscopy (CV-AFS) [9,10], etc. However, some disadvantages have been reported for these techniques, including being time-consuming, requiring sophisticated instruments, and a need for a large volume of samples. Simple and eco-friendly procedures have been developed for the sensitive and specific sensing of $Hg^{2+}$, and they have become greatly desirable to overcome these limitations [11]. In Table S1, the different analytical characteristics of these detection techniques for the quantification of $Hg^{2+}$ are compared.

Fluorescence analysis is a very promising method due to its rapid process, operational simplicity, and high sensitivity. In this regard, numerous fluorescent probes have been fabricated for $Hg^{2+}$ detection, including metal nanoclusters [12–14], fluorescent dyes [15,16], semiconductor quantum dots (QDs) [17–19], and carbon-based quantum dots [20]. Among them, carbon-based quantum dots, especially graphene quantum dots (GQDs) and carbon quantum dots (CQDs), have received special attention owing to their easy synthesis from natural resources, non-toxicity, water solubility, biocompatibility, and excellent optical properties. Moreover, the optical properties of CQDs and GQDs can be tailored by doping with different metals or non-metals. However, due to the toxicity of metal ions and the resulting inefficient and non-uniform doping due to their larger radii than those of carbon atoms, their use is restricted [21]. In comparison, doping CQDs and GQDs with non-metallic heteroatoms such as phosphorus (P), nitrogen (N), sulfur (S), and boron (B) has proven to be an effective means of altering their optical properties, improving their fluorescent quantum yields (QY), and making them more practical tools for a broader range of applications [1,22].

In this review, the synthesis of heteroatom-doped CQDs and GQDs, their QYs, their fluorescence characteristics, and their application as optical probes in the fluorescence sensing of $Hg^{2+}$ have been discussed.

## 2. CQDs and GQDs as Promising Fluorescent Probes

Common fluorescent dyes have inflexible optical properties, low photo stability, and low QY. The alternative way to overcome these limitations is the use of QDs, because they have good photostability with size-tunable optical properties and high quantum efficiency [23]. Conventional metallic and semiconductor QDs are environmentally questionable and seriously toxic, even in relatively low concentrations [11]. Therefore, the demand for non-metallic QDs with sufficient photo stability, easy and inexpensive production, low toxicity, and high fluorescence QY has become a vital challenge. Carbon-based QDs such as CQDs and GQDs meet all these requirements and have become an interesting class of advanced fluorescent probes as they are mainly composed of carbon, a generally non-toxic element, which is likely to offer a notable advantage for their application, particularly in the biological field.

CQDs were discovered accidentally during the purification of single-walled carbon nanotubes (SWNTs) in 2004 and were subsequently named in 2006. CQDs with a size of 1–10 nm, consisting of a core of $sp^2$ graphitic carbon and/or a surface of amorphous carbon shell ($sp^2/sp^3$ carbon) coated with oxygen-rich functional groups, are a great alternative to conventional fluorescent materials, as their functional groups give them high water solubility, high biological activity, and facilitate conjugation with various inorganic and organic substances [24,25]. The optical properties can also vary considerably depending on the choice of synthesis method, passivation, doping, and size of the CQDs.

GQDs composed of $sp^2$-hybridized carbon are QDs with oxygen-containing functional groups at their edges and photoluminescent (PL) properties. Both their height and lateral dimensions are less than 100 nm. They can be manufactured using "top-down" or "bottom-up" procedures. GQDs exhibit unique properties, including variable bandgaps,

the presence of hydroxyl and carboxyl functional groups on their edges and consequently, an ease of functionalization, water solubility, high biocompatibility, a large surface area, chemical inertness, quantum confinement, electrochemical, optical, and electrochemiluminescent characteristics, and are energy size-dependent [26]. Therefore, they have attracted a great deal of research interest, not only in the fluorescence detection of chemical and biological analyte, but also in other application areas like light emitting diodes, photocatalysis, bioimaging, and photovoltaic devices.

## 3. Optical Features of Carbon and Graphene Quantum Dots

CQDs normally demonstrate strong absorption in the ultraviolet (UV) spectral area with a visible stretching absorption tail. Furthermore, a shoulder or a weak peak is sometimes seen at a wavelength that is rather longer than the UV absorption peak. The UV absorption at a shorter wavelength, 200–350 nm, is linked to the π-π* electronic transitions of C=C, which are found in the core of CQDs nanoparticles. UV absorption with a longer wavelength, which normally manifests as a shoulder or a weaker peak of 300–400 nm, is linked to n-π* transitions of C=O on the surface of CQDs and hybridization with heteroatoms like N, S, P, etc. [27]. Moreover, it is possible to tune the absorption properties of CQDs via a modification process or surface passivation. More prominently, the CQDs have uniform fluorescence properties with a wide emission peak range from the ultraviolet to the near-infrared. Their fluorescence properties can be tuned purposefully by monitoring their size, shape, and heteroatom doping, as well as by altering their surfaces and edges due to the remarkable edge effect, quantum confinement, and surface effect [28]. For example, it has been exhibited that the blue fluorescent emission with higher QY can be achieved via N/S/P- functionalization at the edges of the CQDs [29].

The GQDs optical characteristics rely on the presence of surface functional groups, doping, and flaws [30]. GQDs demonstrate two different peaks at the UV-visible region. We can observe a strong peak at ~230 nm and a weak edge at ~300 nm, which originate from aromatic C=C bonds related to π-π* transition and aromatic C=O bonds related to n-π* transition, respectively [30]. Just like CQDs, the absorption spectrum of GQDs strongly depends on the size, synthesis techniques, functionalization, and doping. By reducing the size of GQDs, the absorption peak will be shifted to blue [31]. Remarkably, the absorption spectrum of the GQDs will be altered via various synthesis methods. For instance, hydrothermally synthesized GQDs with a diameter of 9.6 nm show a UV absorption (320 nm) peak similar to solvothermally obtained GQDs with a diameter of 5 nm [32].

Moreover, most GQD materials exhibit blue emissions with low photoluminescence QY, significantly restricting their applications. Additionally, their production processes are often time-consuming and complex. To address this issue, GQD geometry is altered through functionalization at various edge locations, leading to significant red shifts and enhanced electronic localization. This advancement promotes their use as novel two-dimensional nanomaterials for optical tuning [33]. In this context, Tang et al. [34] were able to realize a tunable emission wavelength from 505 nm (cyan) to 560 nm (yellow) via the co-doping of GQDs with N and S (N, S-GQDs) and through further adjusting the concentration of the N, S-GQDs solution (Figure 1). They produced N, S-GQDs using catechol and o-phenylendiamine as the raw substances in a dimethyl sulfoxide solution and under UV irradiation conditions for 2 h. The synthesized N,S-GQDs possessed good crystallinity and uniform size and showed a clear red shift with an increasing concentration of N,S-GQDs.

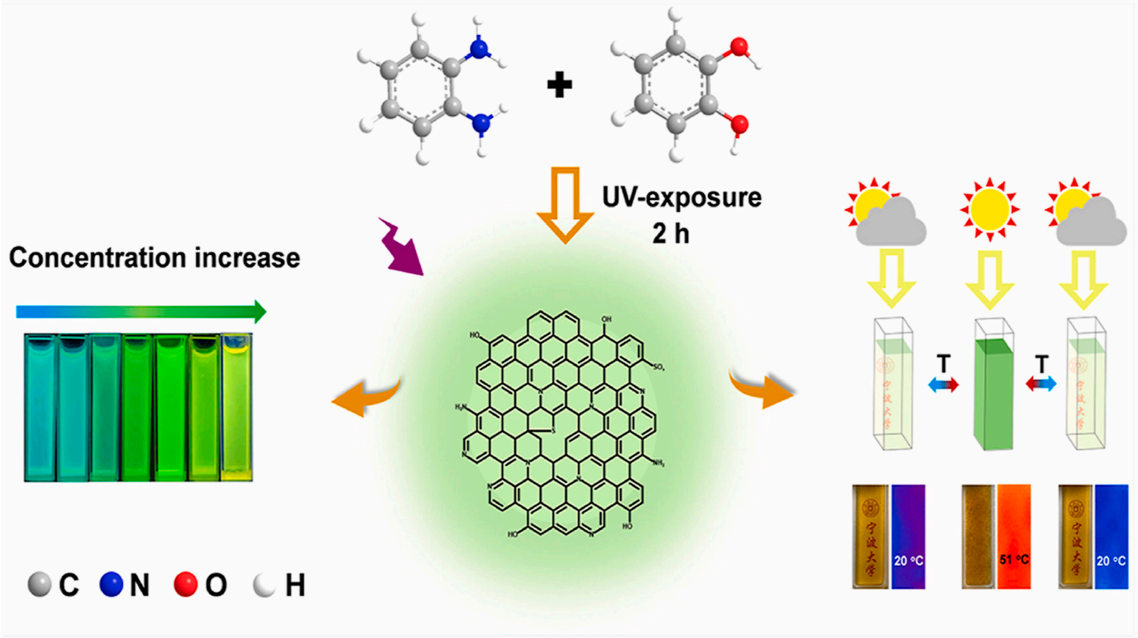


**Figure 1.** Schematic representation of the synthesis of N,S-GQDs via UV irradiation, illustrating the concentration-dependent properties (**left**) and the photothermal conversion process (**right**) [34]. Reprinted with permission from Elsevier.

## 4. Synthesis Methods of Carbon and Graphene Quantum Dots

In recent years, many synthesis strategies (Figure 2) based on both top-down (destroying or dispersing macromolecules into small CQDs via physical or chemical methods) and bottom-up (chemical polymerization and carbonization of small molecules to CQDs) methods for the production of CQDs have been developed and reviewed [28,35–38]. It is therefore not our intention to provide a detailed account of these matters, as more comprehensive information can be found in the relevant reviews.

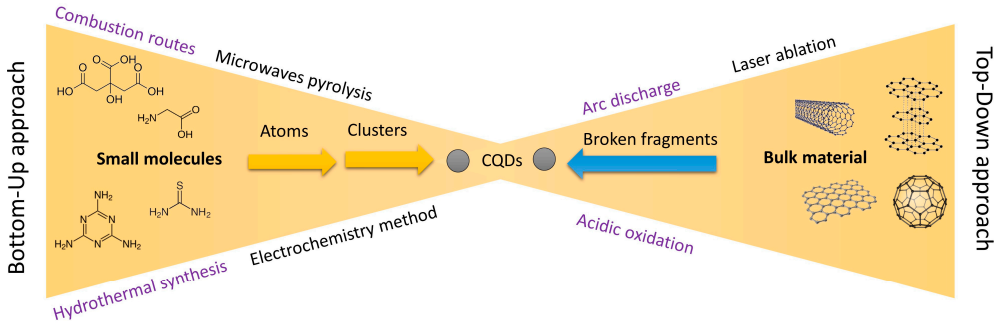


**Figure 2.** Bottom-up and top-down strategies for synthesis of CQDs.

Arc discharge, laser ablation, and electrochemical oxidation processes are employed as top-down approaches that use graphite dust or SWCNTs and multi-walled carbon nanotubes (MWCNTs) as starting materials. These procedures usually require post-processing and a strong acidic or alkaline solution to produce CQDs, but the QY is still not high enough (lower than 10%) and the size of the particles cannot be controlled [20,24]. Hydrothermal/solvothermal, microwave pyrolysis, and ultrasonic synthesis processes are used as bottom-up approaches, in which macromolecular precursors with surface passivation agents, biomass, and materials with carbon sources such as glucose, fructose, chitosan, and chicken eggs are used for CQDs synthesis. Compared to the top-down methods, they do not require harsh reaction conditions and materials. Additionally, the QY is higher, and the size of the produced particles is more controllable and homogeneous. The hydrothermal

method is the most preferred of the aforementioned bottom-up techniques due to its numerous advantages. These include the fact that the synthesis process is both cost-effective and rapid, that environmentally friendly components are utilized (such as orange, coconut and banana peel, rice husk and papaya, among others), and that the particles produced are smaller and more homogeneous with a higher QY [39,40]. For example, Zhu and coworkers could produce the CQDs using citric acid and ethylenediamine with the highest QY of 80 % and average size of 2.81 nm using the hydrothermal method [41]. In another study, Jing et al. produced CQDs with a size of ~2.4 nm and a QY of 76.9% from carbon-derived biomass, including hydrochar and carbonized biomass, through mild oxidation [42].

Similar to the CQDs, the GQDs were synthesized using either top-down or bottom-up approaches (Figure 3), which are reviewed in several papers [43–45]. Chemical and electrochemical oxidation, electron beam lithography, and microwave-assisted hydrothermal, solvothermal, and microfluidization are the top-down methods that utilize graphite [46], graphene and its derivatives (like graphene oxide and graphene nanoribbons) [47–49], carbon nanofibers [50], and carbon black [51] as carbon source materials for GQDs production. However, the application of these top-down processes is limited by some drawbacks, such as the need for special equipment, difficult reaction conditions, and the formation of poorly crystalline and nonhomogeneous GQDs with relatively low QYs. Bottom-up approaches such as microwave hydrothermal, pyrolysis, and oxidation were used to prepare GQDs based on the condensation of smaller units of benzene derivatives [52] as well as biomass waste [53]. Using bottom-up techniques, it is possible to produce homogeneous GQDs with desired sizes, shapes, and properties [43,54]. Nevertheless, a disadvantage of the bottom-up route is the purification of the synthesized GQDs from the starting materials and by-products.

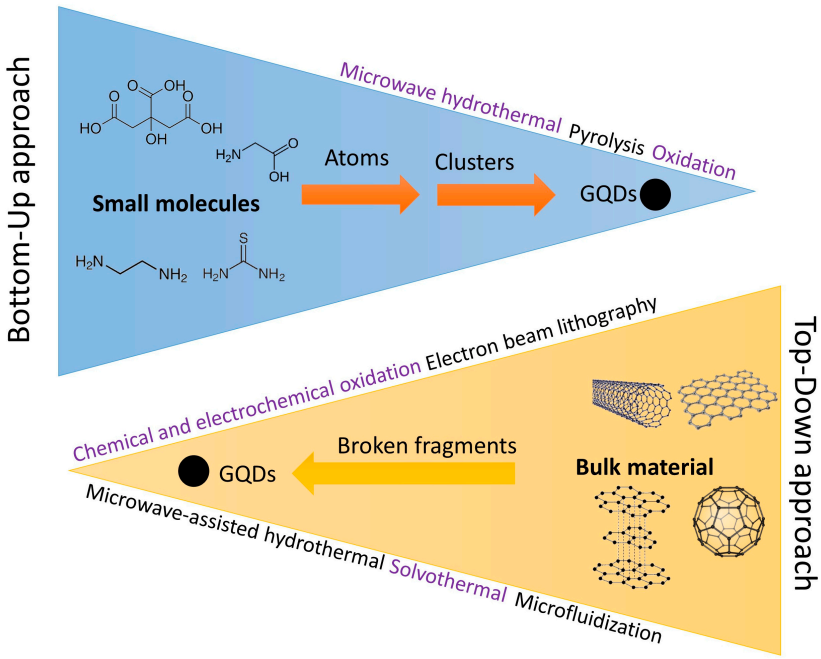


**Figure 3.** Bottom-up and top-down strategies for synthesis of GQDs.

## 5. Doping Carbon and Graphene Quantum Dots with Heteroatoms

Despite the development of numerous straightforward and efficacious synthesis techniques for the fabrication of CQDs and GQDs, the large-scale synthesis of reproducible and controllable CQDs and GQDs with a considerably higher QY comparable to that of semiconductor QDs remains a significant challenge. Consequently, ongoing efforts are directed towards overcoming these limitations through the further surface functionalization, passivation, and doping of CQDs and GQDs. Heteroatom doping is regarded as a

promising strategy to modulate the bandgap and electron density as well as to improve the QY of CQDs and GQDs due to their inherent scalability, simplicity, and low cost [44]. Among the various heteroatom dopants, N and S are the most commonly used elements for CQDs doping, because they have similar electronegativity and a comparable atomic size, as well as strong valence bonds [55]. It has been theoretically and experimentally investigated that N- and S-doping introduces additional electron pairs and consequently more new defects on the surface of CQDs/GQDs and induces the formation of more $sp^2$-hybridized sites, leading to an enhancement of fluorescence. Moreover, the band gap between the lowest unoccupied molecular orbitals (LUMO) and the highest occupied molecular orbitals (HOMO) is reduced, which has a positive effect on fluorescence enhancement [55–58].

In the case of N-doping, due to the similar size and structure of N and C, doping amplifies the surface defects of CQDs/GQDs and introduces more reactive groups (such as N=C, CN, $NH_2$), which leads to an improvement in the electrical and optical properties. Therefore, it has been adopted as the most commonly used doping-strategy for improving the fluorescence properties of CQDs/GQDs. As an example, Cheng et al. produced nitrogen-doped CQDs (N-CQDs) using urea and citric acid hydrothermal treatment (Figure 4). The obtained N-CQDs show a high relative QY of 82.4% in a wide-range pH from 4 to 9, good fluorescence stability, and strong blue luminescence [59]. In another study, Luo et al. [60], using the hydrothermal technique and 2,4,6-triaminopyrimidine as the precursor, synthesized the CQDs containing 41% nitrogen with a bright blue fluorescence and a QY of 74.9%. Guo et al. used a one-step solvothermal molecule fusion method to introduce amine functional groups onto atomic-Fe-rich CQDs as photocatalysts. They feature an impressive Fe-loading capability and well-defined Fe-$N_4$ active sites that causes a synergistic effect between their electron-donating amine functional groups and Fe-$N_4$ active centers, enabling an outstanding $CO_2$-to-CO conversion performance and inhibiting a photocatalytic reduction in$CO_2$ to CO [61].

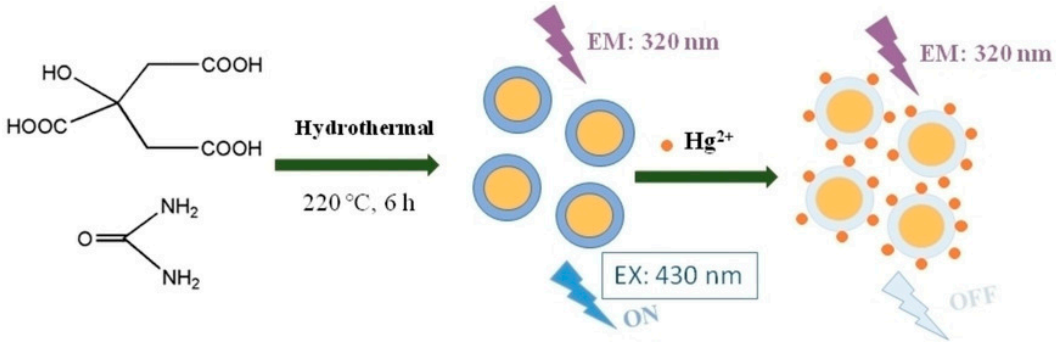


**Figure 4.** Nitrogen-doped carbon quantum dots as "turn-off" fluorescent probes for highly selective and sensitive detection of mercury (II) ions [59]. Reprinted with permission from Wiley.

In contrast, S-doping is more difficult due to the larger size of the S atom compared to the carbon (C) atom and the small difference in electronegativity of both atoms, so that a significant charge transfer seems almost impossible between C-S [62]. This is despite the fact that there are several reports on the synthesis of S-doped CQDs/GQDs, where S-doping has improved the electronic and optical properties as well as the surface chemical reactivities of CQDs/GQDs. This improvement can be attributed to the electron-rich nature of the S atom, which increases the electron-donating ability of the CQDs/GQDs [63–66]. Thiophene structures can create GQDs containing S atoms with good chemical stabilities and optical properties, and ultrahigh QY [2].

Shen et al. reported oxygen-doped CQDs (O-CQDs) that demonstrated amazing selectivity and outstanding performance as electrocatalysts for $H_2O_2$ production [67]. Experimental results reveal that the introduction of a series of functionalized GQDs during the synthesis of near-atom layer 2H-$MoS_2$ nanosheets remediated with GQDs plays a crucial role in this process [68].

## 6. Using Carbon and Graphene Quantum Dots for Quantitative Analysis

The unique optical properties of CQDs make them excellent candidates for quantitative analysis. Typically, CQD-based fluorometric sensing can be structured in both turn-on and turn-off modes. In the turn-off mode, the interaction between CQDs and specific analytes leads to quenching, resulting in a reduction in the emitted fluorescence. Conversely, in the turn-on mode, this interaction enhances the fluorescence emission of the CQDs [25]. The turn-off and turn-on modes provide versatile approaches for designing fluorometric sensing systems based on CQDs, allowing for the detection and quantification of various analytes like metal ions [69–71], drugs [72,73], explosives [74,75], pesticides [76–78], small organic molecules [2,79,80], proteins [81,82], nucleic acids [83], and bacteria [44,84,85] through distinct fluorescence responses. Indeed, the turn-off sensing process has encountered challenges due to background fluorescence interference, making it less practical in sensing applications. However, to address this limitation, a recent introduction of an on-off-on switching strategy shows significant promise. This innovative approach holds great potential to create highly sensitive sensing platforms capable of detecting trace amounts of desired analytes [86,87].

The selection of appropriate precursors for CQDs preparation allows the creation of a finely tuned probe with high selectivity, sensitivity, and linearity between CQDs fluorescence intensity and analyte concentration. In the CQD-based fluorescence sensing of metal ions, the mechanism often involves electron transfer from chelation between the metal ions and the surface functional groups of the CQDs. This interaction leads to changes in fluorescence intensity, which is the basis for detecting and quantifying the presence of specific metal ions in a sample [88]. To date, various fluorometric sensors have been successfully developed for $Hg^{2+}$ detection based on simple CQDs, heteroatom-doped CQDs, and modified CQDs, as summarized in Table 1 [1,3].

**Table 1.** Developed fluorometric sensors based on CQDs for $Hg^{2+}$ detection.

| CQDs Precursor | Synthesis Method | QY | LOD | Linear Range | Reference |
|---|---|---|---|---|---|
| Citric acid, tartaric acid, ethanediamine | Solvothermal | - | 83.5 nM | 0–18 µM | [1] |
| Citric acid, melamine | Solid thermal method | - | 0.44 µM | 2–14 µM | [3] |
| Citric acid, ethylenediamine, $Mg(OH)_2$ | Hydrothermal | - | 0.02 µM | 0.05–5 µM | [24] |
| Citric acid, glutathione or thiourea | Microwave hydrothermal | 26% | 5.4 µM | 5–50 µM | [25] |
| Citric acid, urea | Hydrothermal | - | 1.3 nM | 0.005–250 µM | [59] |
| Citric acid, L-cysteine, | Hydrothermal | - | 4.2 pM | 0.01–0.75 nM | [88] |
| Citric acid, triethylenetetramine, (TETA) | Thermal | 54% | 0.2 nM | 1–20 nM | [89] |
| Citric acid, ethylene diamine | Hydrothermal | - | - | - | [90] |
| Citric acid, 2,2-dimethyl-1,3-propanediamine | Microwave-assisted synthesis | 51.20% | 7.63 nM | 0–4.2 µM | [91] |
| Citric acid, urea | Hydrothermal | - | 8.7 µM | 10–70 µM | [92] |
| Citric acid, glycine | Hydrothermal | - | 38 ppb | 0.12–2 ppm | [93] |
| Citric acid, spermine | Hydrothermal | - | 2.2 nM | 0.01–1.0 µM | [94] |
| Citric acid, aminopropyltriethoxysilane (APTEOS) | Hydrothermal | | 0.015 µM | 0.02–5.0 µM | [95] |
| Citric acid, chitosan, thiourea | Hydrothermal | 33.00% | 4 nM | 5–160 nM | [96] |
| 2,4,6-Triaminopyrimidine | Hydrothermal metho. | - | 11.4 nM | - | [60] |
| Xylose | Solvothermal | - | 10 nM | 50–800 nM | [97] |
| Glutathione | Solvothermal | 41.90% | 0.5 µM | 0.5–15.0 µM | [98] |
| Ortho-phenylenediamine (OPDA) | Solvothermal | - | 60 nM | 30–60 µM | [99] |
| Methyl orange | - | 29.4 | 237 nM | - | [100] |

**Table 1.** *Cont.*

| CQDs Precursor | Synthesis Method | QY | LOD | Linear Range | Reference |
|---|---|---|---|---|---|
| Malic acid, urea | Microwave-assisted hydrothermal synthesis | - | 0.90 μM | 0–40 μM | [101] |
| Trisodium citrate dihydrate, DL-thioctic acid, | Hydrothermal | - | 33.3 nM | 0.05–5.8 μM | [102] |
| Aconitic acid, oligomeric polyethyleneimine | Thermal | 44.20% | 84 nM | 0–800 μM | [103] |
| Polyamidoamine (PAMAM), and (3-aminopropyl)triethoxysilane (APTES) | Hydrothermal | - | 87 fM | 0.2 nM–10 μM | [104] |
| Diaminomaleonitrile (DAMN), thymine-1-acetic acid | Microwave-assisted hydrothermal synthesis | - | 0.15 nM | 1.0–500 nM | [105] |
| Glucose, $HAuCl_4$, reduced glutathione | Microwaving | - | 8.7 nM | 50–1000 nM | [2] |
| Glucose, boric acid, thiourea, phosphoric | Hydrothermal | - | 16.5 μM | 25.0 μM–1500.0 mM | [106] |
| Trisodium citrate dihydrate, melamine | Microwave-assisted hydrothermal | - | 42 nM | 0–6 μM | [107] |
| Methyl glycine diacetic acid trisodium salt (MGDA), m-phenylenediamine (MPD) | Hydrothermal | 63.8 | 0.9 μM | 0–100 μM | [68] |
| D-Glucose, aspartic acid, and branched polyethyleneimine | Hydrothermal | - | 10 nM | 20–800 nM | [108] |
| Honey | Hydrothermal | - | 1.02 nM | 0–10 nM | [11] |
| Tamarindus indica leaves | - | - | 6 nM | 0–0.1 μM | [20] |
| Hongcaitai | Hydrothermal | - | 0.06 μM | 0.2–15 μM | [72] |
| Black wolfberry | Hydrothermal | - | 0.12 nM | 0–300 μM | [109] |
| Highland barley, Ethylenediamine | Hydrothermal | 14.40% | 0.48 μM | 10–160 μM | [110] |
| Peach palm (Bactris gasipaes) peels | Microwave assisted | 25.4 | 0.19 μM | - | [111] |

As illustrated in Table 1, citric acid is recognized as a highly prevalent precursor in conjunction with other suitable precursors in the synthesis of CQDs through a bottom-up approach. The majority of the employed precursors in combination with citric acid for the synthesis of CQDs are utilized for the purpose of doping N and S heteroatoms in the structure of CQDs. Additionally, complex compounds comprising heavy molecules [108] or bulk structures [11] have been documented in the preparation of CQDs via top-down approaches. As evidenced by the data presented in Table 1, a variety of strategies have been employed in the synthesis or modification of CQDs with the objective of achieving optimal sensor performance. These strategies include the use of novel materials, modifications, redesigned sensors, and other innovative techniques, with the aim of developing a highly effective procedure for the detection of Hg, either alone or in conjunction with other analytes.

The highly sensitive and selective fluorescence quenching of N-, S-, doped CQDs, and N, S- co-doped CQDs by $Hg^{2+}$ can be attributed to two primary mechanisms. First, $Hg^{2+}$, due to its larger ionic radius and stronger chemical interaction with functional groups of doped CQDs, easily forms stable, non-fluorescent complexes. Second, the quenching may result from the aggregation of doped/co-doped CQDs, where $Hg^{2+}$ simultaneously binds to multiple nitrogen and oxygen atoms in the doped/co-doped CQDs. This complexation induces aggregation, leading to changes in the electronic structure of doped/co-doped CQDs and ultimately quenching their fluorescence.

Han et al. employed a strategy to design a highly sensitive sensor for $Hg^{2+}$ detection by functionalizing CQDs with sulfhydryl groups (HS-CQDs), which have a high affinity for the target metal ions, mediated by $Ag^{+}$. The sensing mechanism (Figure 5) involved quenching the fluorescence of HS-CQDs through the induced agglomeration caused by adding $Ag^{+}$, and then restoring the fluorescence by adding $Hg^{2+}$. The higher affinity between -SH

and $Hg^{2+}$ results in the substitution of $Hg^{2+}$ for $Ag^{+}$ in the CQDs/Ag agglomerate and a subsequent amalgamation. This design provided the sensor with a linear detection range of 0.01 to 0.75 nM and an ultra-low detection limit of 4.2 pM for $Hg^{2+}$ [88].

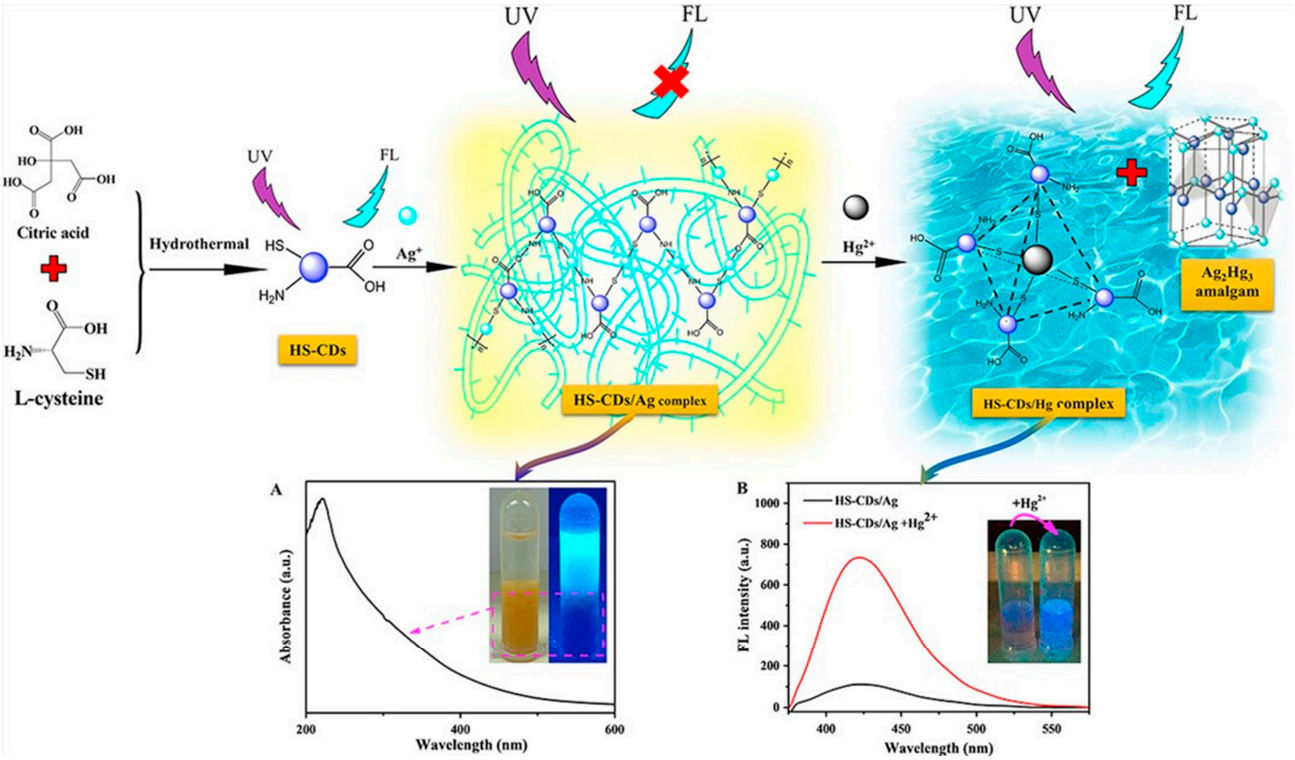


**Figure 5.** Fluorescent sensing method to determine $Hg^{2+}$ in aqueous solutions using sulfhydryl functionalized CQDs (HS-CQDs) mediated by $Ag^{+}$. (**A**) Absorption spectrum of the HS-CDs/Ag precipitate; the insets are corresponding photos of HS-CQDs/Ag under visible light (**left**) and UV light at 365 nm (**right**). (**B**) FL spectra of HS-CDs/Ag and HS-CQDs/Ag + $Hg^{2+}$; the insets are corresponding photos of the HS-CQDs/Ag sensor (**left**) and the HS-CQDs/Ag $^{+}$ $Hg^{2+}$ (**right**) under UV light at 365 nm [88]. Reprinted with permission from Elsevier.

To design a more sensitive sensor for Hg, a dual-emission fluorescence strategy was developed by modifying CQDs with Europium (III, $Eu^{3+}$) [89]. This involved combining blue-emissive CQDs (at 443 nm) with red-emissive europium complexes (at 617 nm) to create the new dual-emission fluorescence approach. The addition of $Hg^{2+}$ to the designed sensor resulted in a notable enhancement in dual-emission fluorescence intensity. As the concentration of $Hg^{2+}$ increased, the sensing platform exhibited a discernible change in color, from a deep blue to a light blue, then to a lavender hue, and finally to a deep purple. The sensor displayed remarkable sensitivity and selectivity towards $Hg^{2+}$, with a linear concentration range of 1 to 20 nM and a LOD of 0.2 nM. This procedure was effectively applied for the ultrasensitive and visual sensing of $Hg^{2+}$ in milk and drinking water samples with acceptable recovery from 97.6% to 105.4%.

Guo et al. introduced another dual-emission ratiometric fluorescent system for $Hg^{2+}$ detection by embedding CQDs into europium metal–organic frameworks (Eu-MOF) using a straightforward in situ hydrothermal method [109]. The proposed fluorescence composite material, which exhibited good stability in an aqueous solution while possessing the excellent luminescence properties of $Eu^{3+}$ and CQDs, was successfully employed to detect $Hg^{2+}$ in environmental water samples. In this system, the fluorescence of the encapsulated CQDs within the Eu-MOF was significantly quenched by $Hg^{2+}$, while the fluorescence emission of the Eu-MOFs remained unaffected. This dual-functionality, providing both a recognition part (CQDs) and a reference part (Eu-MOF), offers a distinct advantage for

constructing a ratiometric fluorescence sensor for $Hg^{2+}$ detection in aqueous solutions. The developed sensor demonstrated an excellent response to $Hg^{2+}$ over a wide linear range (0–300 μM) with a lower detection limit of 0.12 nM, surpassing the performance of a previously reported ratiometric fluorescence system [89].

In a further strategy for the rapid and ultrasensitive co-analysis of $Hg^{2+}$ and $Pb^{2+}$ based on photoluminescence and magnetic properties, Ahmadian-Fard-Fini and colleagues proposed combining CQDs, nanofibers, and magnetic nanoparticles [90]. The CQDs were initially prepared via a hydrothermal method, utilizing citric acid (from lemon extract) and ethylene diamine as precursors. The magnetic nanoparticles were then synthesized through ball milling, while the cellulose acetate nanofibers were produced through electrospinning. To construct the magnetic nanofiber fluorescent sensor, the magnetic nanoparticles were incorporated into the polymeric cellulose nanofibers. Subsequently, the CQDs were coated onto the fibers through a sonochemical-assisted hydrothermal method. Following the exposure of the designed sensor to $Hg^{2+}$ and $Pb^{2+}$, a reduction in the photoluminescent intensity (blue color) of the CQDs was observed. This reduction occurs because electrons from the excited CQDs are transferred to the d-orbitals of $Pb^{2+}$ and $Hg^{2+}$, leading to the formation of a complex.

In another study, Muthurasu and Ganesh reported a ratiometric sensing strategy for Hg using a hybrid system in which N-CQDs serve as the donor and Rhodamine B as the acceptor [92]. The intermolecular interaction between N-CQDs and Rhodamine B enables effective fluorescence resonance energy transfer (FRET), leading to a tunable shift in the fluorescence emission color of N-CQDs from blue to red. Interestingly, varying the concentration of Rhodamine B resulted in different emission colors, and the concentration that emitted violet fluorescence was selected for the sensing experiments. The addition of varying concentrations of $Hg^{2+}$ ions effectively quenched the photoluminescence properties of N-CQDs due to the complexation of $Hg^{2+}$ with the carboxylic acid and amine functional groups present in N-CQDs. In contrast, no interaction was detected for RhB with $Hg^{2+}$ ions.

In a recent study, Lu et al. developed a dual-mode sensing platform for the colorimetric and turn-on fluorometric detection of $Hg^{2+}$. This platform was based on the modification of N-CQDs with a sulfhydryl group (–SH) and their subsequent combination with gold nanoparticles (AuNPs). Following the integration of SH-modified N-CQDs, a reduction in fluorescence intensity was observed, which was attributed to the fluorescence quenching effect of AuNPs. But, upon the addition of $Hg^{2+}$, the fluorescence intensity of the SH-modified N-CQDs was gradually restored, accompanied by a visible color change, transitioning from red to blue-violet, and eventually to blue. The sensing mechanism could be explained as follows: Initially, the fluorescence of SH-modified N-CQDs was quenched due to their strong interaction with AuNPs. When $Hg^{2+}$ was introduced, citrate ions on the surface of the AuNPs reduce $Hg^{2+}$ to $Hg^{0}$. This reduction leads to the formation of a gold–mercury alloy through Hg–Au metallophilic interactions on the AuNP surface. As $Hg^{0}$ occupies the surface, the modified N-CQDs were released, resulting in the restoration of their fluorescence. Furthermore, to emphasize the significance of the modification of N-CQDs with the SH group in the sensing performance of the proposed sensor, they presented a sensor based on unmodified N-CQDs with AuNPs. It was observed that under visible light, SH-modified N-CQDs did not affect the color of AuNPs. However, unmodified N-CQDs were found to cause the color of AuNPs to change from red to bluish violet, which interfered with the determination of $Hg^{2+}$ through the use of a color reaction. This finding confirmed the crucial role of the SH functional group on CQDs in enhancing their optical properties and contributing to the development of a sensitive and selective Hg sensor [98].

Building on the observed increase in QYs and fluorescence properties after doping and functionalizing CQDs, an attempt was made to dope CQDs with S using thioctic acid, chosen for its strong chelating properties with metal ions [102]. The sensing mechanism relied on the quenching of S-doped CQDs fluorescence upon exposure to $Hg^{2+}$ ions, attributed to electron transfer between $Hg^{2+}$ and the S-doped CQDs, leading to complex formation (turn-off). The fluorescence was then restored (turn-on) by adding thiophanate

methyl, which forms thiophanate methyl-Hg complexes due to the strong affinity between $Hg^{2+}$ and the two mercapto groups in thiophanate methyl. Based on this mechanism, the proposed sensor demonstrated dual functionality, enabling the detection of both $Hg^{2+}$ ions and thiophanate methyl, a systemic fungicide. Under optimal conditions, the fluorescence sensor system achieved limits of detection of 7.6 nM for thiophanate methyl and 33.3 nM for $Hg^{2+}$. Consequently, the developed sensor can be utilized as a multifunctional tool for monitoring trace contaminants in the environment and ensuring the quality control of food safety products.

Ge et al. developed a reusable sensor for detecting Hg and Cu using functionalized CQDs synthesized with aconitic acid for core carbon nanoparticle formation and oligomeric polyethyleneimine as a functionalization agent [103]. The fluorescence of the prepared CQDs was effectively quenched upon the addition of $Cu^{2+}$ or $Hg^{2+}$ across a broad linear concentration range, achieving low detection limits of 70 nM for $Cu^{2+}$ and 84 nM for $Hg^{2+}$. Additionally, the sensor could be regenerated by introducing aspartic acid or L-cysteine, which serve as metal ion chelators, forming complexes with the metal ions. It is important to note that the proposed "on–off–on" sensing system can be utilized not only for the detection of $Hg^{2+}$ and $Cu^{2+}$ but also for aspartic acid and L-cysteine.

GQDs have gained prominence as other carbon-based fluorescence materials due to their exceptional optical properties, high QY, and unique characteristics. Their excellent photoluminescence, high stability, and tunable properties make them promising candidates for various applications, particularly in sensing and biosensing. GQDs present analogous advantages to CQDs and have gained attention as valuable substitutes in fluorescence-based sensor technologies. Due to various interactions such as electrostatic interaction or electron transfer as well as π-π* conjugation between GQDs and the target analyte, the fluorescence intensity of the GQDs is modulated either by quenching (switch-off mode) or through enhancement mechanisms (switch-on mode) and used as a sensor response [46,112,113]. Similar to CQDs, fluorescence-based sensors based on GQDs using the "on-off-on" fluorescence switching mode have been proposed for the ultrasensitive and selective detection of various analytes, especially for metal ions, as well as for simultaneous multi-analytes detection [114–116]. Various developed fluorometric sensors and biosensors based on GQDs for the detection of $Hg^{2+}$ and their sensing performance are compared and showed in Table 2. As indicated in Table 2, the studies conducted in relation to the fabrication of GQDs are based on bottom-up [117] and top-down methods [118]. In the bottom-up approach, citric acid and glucose are the most frequently used carbon sources for the synthesis of GQDs. In contrast, the top-down procedure has predominantly employed graphene oxide (GO) for the production of GQDs.

**Table 2.** Developed fluorometric sensors based on GQDs for $Hg^{2+}$ detection.

| GQDs Precursor | Synthesis Method | QY | LOD | Linear Range | Reference |
|---|---|---|---|---|---|
| Glucose, urea, and ammonia sulfate | Infrared (IR)-assisted pyrolysis | - | 10 ppb | 10 ppb–10 ppm | [117] |
| Citric acid and Thiourea | Hydrothermal | 41.90% | 0.14 nM | 0.1–15 µM | [119] |
| Citric acid and ethylene diamine | Hydrothermal | - | 0.45 nM | 100–1000 nM | [120] |
| Citric acid and Gly | Hydrothermal | 35.50% | 8.3 nM | 0–3.0 µM | [121] |
| Graphene oxide | Electrochemical | - | 2.5 µM | 2.5–800 µM | [118] |
| Graphene oxide and 5,10,15,20-tetrakis(1-methyl-4-pyridinio)porphyrin tetra(p-toluenesulfonate) (TMPyP) | Two-step hydrothermal method | - | 0.32 nM | 2–200 nM | [122] |
| Graphene oxide, urea, citric acid | Solvotermal | - | - | - | [123] |

In a pioneering study, Gue and colleagues reported the development of a $Hg^{2+}$ fluorescence sensor utilizing S and N co-doped GQDs. This sensor was synthesized through a rapid IR approach, whereby citric acid and ammonium sulfate underwent thermal pyrolysis under IR irradiation [117]. In order to evaluate the effectiveness of S,N co-doping in GQDs in comparison to N-doped GQDs, the sensing performance of both types was examined across a $Hg^{2+}$ concentration range of 10 ppb to 10 ppm. The findings demonstrated that the sensitivity of the co-doped GQDs was 4.23 times greater than that of the N-doped GQDs. This augmented sensitivity could be ascribed to the coordination of sulfur with the phenolic groups at the edges of the S,N co-doped GQDs, which induced a reduction or interruption of photon injection pathways, resulting in notable fluorescence quenching.

In another study, S,N co-doped GQDs were synthesized using a one-pot hydrothermal method to develop a $Hg^{2+}$ sensor [115]. The doping with N was found to enhance the QY, while the introduction of S improved the selectivity for $Hg^{2+}$ detection through strong coordination interactions. Moreover, S,N co-doped GQDs were coated onto cellulose filter paper strips, which were then utilized as a simple sensor for the rapid and in situ screening of $Hg^{2+}$ in wastewater, yielding satisfactory results.

To enhance the QY and sensitivity of GQDs towards $Hg^{2+}$, Zhu et al. proposed a two-step strategy for the synthesis and subsequent functionalization of GQDs [121]. In this context, GQDs were first synthesized by pyrolyzing citric acid and then functionalized with glycine under alkaline conditions. This process involved a carbamate reaction between the GQDs and glycine, resulting in the successful covalent attachment of glycine to the GQDs, forming Gly-GQDs. Furthermore, the prepared Gly-GQDs revealed an enhanced sensitive and selective detection ability for $Hg^{2+}$ in aqueous solutions and a LOD of 8.3 nM was obtained.

As previously mentioned, while bottom-up techniques are generally preferred over top-down methods, there are a few reports on the fabrication of GQDs using top-down approaches, primarily involving graphene oxide (GO) but employing various preparation techniques, as detailed in Table 2. For example, Liu et al. successfully produced N-doped GQDs in a single step using an electrochemical method in the presence of ammonium hydroxide. They subsequently designed a sensor for $Hg^{2+}$ detection, which exhibited excellent sensing performance across a wide concentration range of $Hg^{2+}$ [118].

Peng et al. introduced an innovative sensing strategy for the detection of trace levels of $Hg^{2+}$ [122]. It was found that the incorporation rate of porphyrin and small $Mn^{2+}$ ions was markedly increased in the presence of trace N-doped GQDs (NGQD) and nanomolar concentrations of $Hg^{2+}$ (Figure 6). The proposed synergistic mechanism posits that the larger $Hg^{2+}$ ions deform the porphyrin nucleus, thereby rendering it more susceptible to the smaller $Mn^{2+}$ ions delivered by the NGQDs. The formation of the metalloporphyrin resulted in a red-shift in the absorption and fluorescence quenching of the porphyrin, while the fluorescence of the NGQDs was gradually enhanced due to the inner filter effect of the porphyrin on the NGQDs. This unique phenomenon was used to develop sensitive and selective ratiometric fluorescence and colorimetric methods for the determination of trace $Hg^{2+}$.

A FRET sensing system has been recently introduced, employing a combination of GQDs as the donor and carbon nanodots (CDs) as the acceptor for the quantification of arsenic ($As^{5+}$) and $Hg^{2+}$. The system takes advantage of the excellent spectral overlap between the emission profile of the GQDs and the absorption profile of the CDs, making them an ideal FRET pair. Upon the addition of $As^{5+}$ and $Hg^{2+}$, the FRET signal was significantly quenched due to the strong affinity of these metal ions to the carboxylic groups on both GQDs and CDs. Furthermore, the fluorescence lifetime of the FRET system decreased from 2.93 ns to 0.44 ns and 1.97 ns in the presence of $As^{5+}$ and $Hg^{2+}$, respectively, confirming the effectiveness of this sensing system [123].

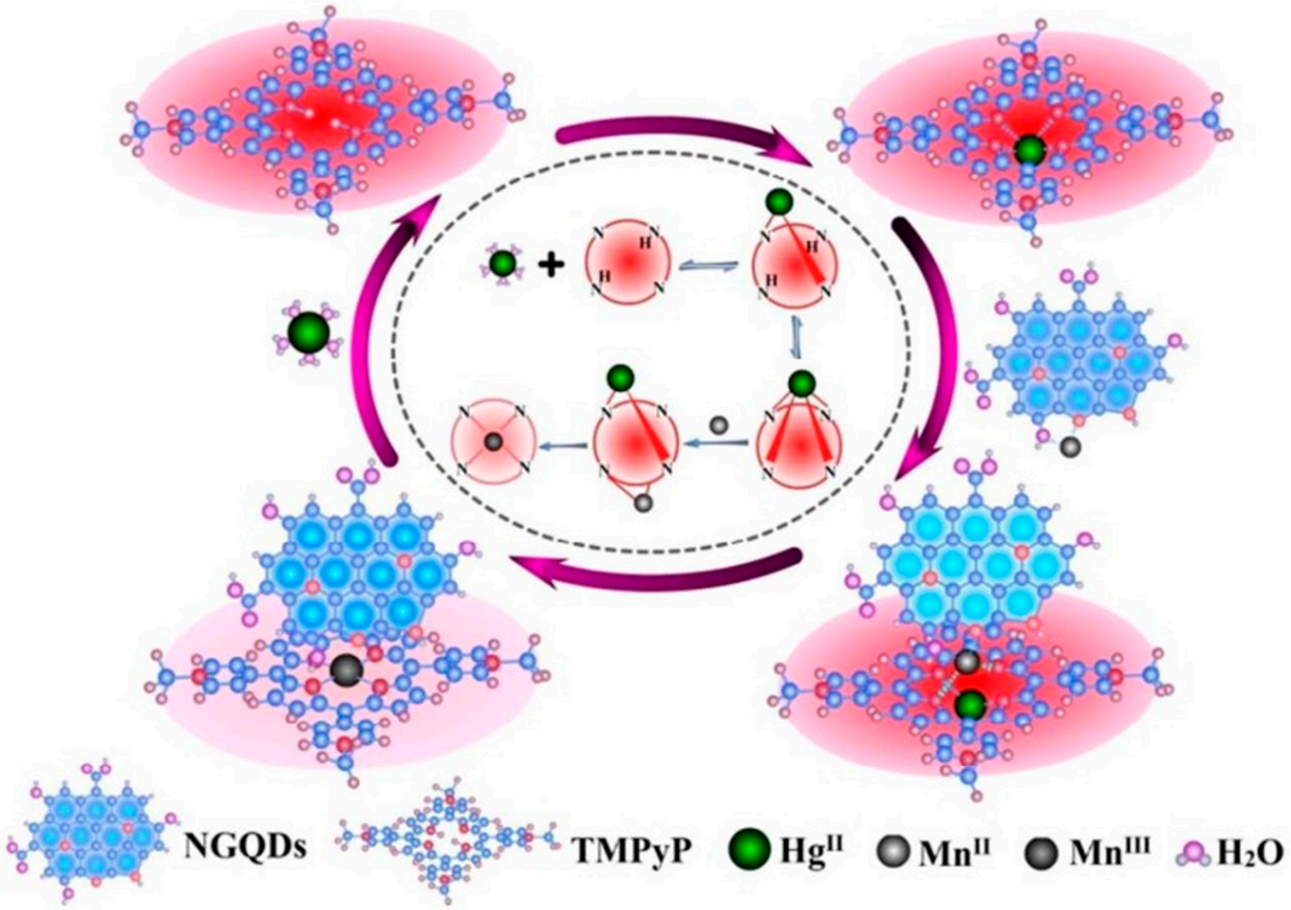


**Figure 6.** The scheme illustration of the synergistic effect of $Hg^{2+}$ and NGQDs in accelerating the coordination rate of $Mn^{2+}$ and 5,10,15,20-tetrakis(1-methyl-4-pyridinio) porphyrin tetra(p-toluenesulfonate) (TMPyP) [122]. Reprinted with permission from ACS.

## 7. Conclusions

$Hg^{2+}$ ranks among the most toxic cations in the environment, posing a significant risk to human health. Therefore, developing a sensitive and specific method for detecting $Hg^{2+}$ at trace levels is both critically important and challenging. Among the various proposed techniques, fluorometric sensors are notable for their simplicity, rapid sample preparation, and quick response times. In particular, fluorometric sensing assays utilizing GQDs and CQDs demonstrate considerable potential for determining and monitoring heavy metals, thanks to their unique optical, chemical, and physical properties. These nanomaterials can be synthesized using various top-down and bottom-up methods. However, studies indicate that bottom-up methods for producing CQDs and GQDs are preferred over top-down approaches, as they avoid harsh reaction conditions and yield particles with higher QY and more uniform sizes. Furthermore, the optical properties of CQDs and GQDs can be tailored through doping and functionalization, which subsequently enhances their sensing performance. In this context, doping with heteroatoms such as N and S, as well as co-doping with both N and S, has been predominantly utilized in $Hg^{2+}$ sensors to enhance the electronic and optical properties of CQDs and GQDs, as discussed in this review. In addition, a range of strategies, including the use of new materials, modifications, redesigned sensors, and other innovative techniques, have been reviewed and debated, all of which aimed at developing highly effective methods for detecting $Hg^{2+}$, both individually and in combination with other analytes.

**Supplementary Materials:** The following supporting information can be downloaded at https://www.mdpi.com/article/10.3390/photonics11090841/s1, Table S1: Comparing the analytical characteristics of different detection techniques for quantifying $Hg^{2+}$.

**Author Contributions:** M.C.: Writing—original draft, investigation, visualization, conceptualization. S.K.: Investigation, writing—review and editing, supervision, project administration. M.N.: Writing—review and editing, supervision, project administration, conceptualization. K.O.: Writing—review and editing, visualization. Y.J.: Writing—review and editing, visualization. P.R.: Writing—review and editing, conceptualization, visualization. All authors have read and agreed to the published version of the manuscript.

**Funding:** This research received no external funding.

**Institutional Review Board Statement:** Not applicable.

**Data Availability Statement:** Data are contained within the article.

**Conflicts of Interest:** The authors declare no conflicts of interest.

## References

1. Huang, H.; Weng, Y.; Zheng, L.; Yao, B.; Weng, W.; Lin, X. Nitrogen-doped carbon quantum dots as fluorescent probe for "off-on" detection of mercury ions, L-cysteine and iodide ions. *J. Colloid Interface Sci.* **2017**, *506*, 373–378. [CrossRef] [PubMed]
2. Wang, G.; Guo, Q.; Chen, D.; Liu, Z.; Zheng, X.; Xu, A.; Yang, S.; Ding, G. Facile and Highly Effective Synthesis of Controllable Lattice Sulfur-Doped Graphene Quantum Dots via Hydrothermal Treatment of Durian. *ACS Appl. Mater. Interfaces* **2018**, *10*, 5750–5759. [CrossRef]
3. Pajewska-Szmyt, M.; Buszewski, B.; Gadzała-Kopciuch, R. Carbon dots as rapid assays for detection of mercury (II) ions based on turn-off mode and breast milk. *Spectrochim. Acta Part A Mol. Biomol. Spectrosc.* **2020**, *236*, 118320. [CrossRef] [PubMed]
4. Ghaedi, M.; Reza Fathi, M.; Shokrollahi, A.; Shajarat, F. Highly selective and sensitive preconcentration of mercury ion and determination by cold vapor atomic absorption spectroscopy. *Anal. Lett.* **2006**, *39*, 1171–1185. [CrossRef]
5. Lee, S.H.; Suh, J.K. Determination of mercury in tuna fish tissue using isotope dilution-inductively coupled plasma mass spectrometry. *Microchem. J.* **2005**, *80*, 233–236.
6. Krata, A.; Vassileva, E.; Bulska, E. Reference measurements for total mercury and methyl mercury content in marine biota samples using direct or species-specific isotope dilution inductively coupled plasma mass spectrometry. *Talanta* **2016**, *160*, 562–569. [CrossRef]
7. KopyŚĆ, E.; PyrzyŃslka, K.; Garbos, S.; Buska, E. Determination of mercury by cold-vapor atomic absorption spectrometry with preconcentration on a gold-trap. *Anal. Sci.* **2000**, *16*, 1309–1312. [CrossRef]
8. Pourreza, N.; Ghanemi, K. Solid phase extraction of cadmium on 2-mercaptobenzothiazole loaded on sulfur powder in the medium of ionic liquid 1-butyl-3-methylimidazolium hexafluorophosphate and cold vapor generation–atomic absorption spectrometric determination. *J. Hazard. Mater.* **2010**, *178*, 566–571. [CrossRef]
9. Erxleben, H.; Ruzicka, J. Atomic Absorption Spectroscopy for Mercury, Automated by Sequential Injection and Miniaturized in Lab-on-Valve System. *Anal. Chem.* **2005**, *77*, 5124–5128. [CrossRef]
10. Pfeil, D.L.; Bruce, M.L. Automated determination of mercury cold vapor atomic fluorescence with gold amalgamation. *Am. Lab.* **2001**, *33*, 26–33.
11. Srinivasan, K.; Subramanian, K.; Murugan, K.; Dinakaran, K. Sensitive fluorescence detection of mercury (II) in aqueous solution by the fluorescence quenching effect of $MoS_2$ with DNA functionalized carbon dots. *Analyst* **2016**, *141*, 6344–6352. [CrossRef] [PubMed]
12. Li, S.; Cao, W.; Kumar, A.; Jin, S.; Zhao, Y.; Zhang, C.; Zou, G.; Wang, P.C.; Li, F.; Liang, X.-J. Highly sensitive simultaneous detection of mercury and copper ions by ultrasmall fluorescent DNA–Ag nanoclusters. *New J. Chem.* **2014**, *38*, 1546–1550. [CrossRef]
13. Nain, A.; Tseng, Y.-T.; Lin, Y.-S.; Wei, S.-C.; Mandal, R.P.; Unnikrishnan, B.; Huang, C.-C.; Tseng, F.-G.; Chang, H.-T. Tuning the photoluminescence of metal nanoclusters for selective detection of multiple heavy metal ions. *Sens. Actuators B Chem.* **2020**, *321*, 128539. [CrossRef]
14. Panthi, G.; Park, M. Synthesis of metal nanoclusters and their application in $Hg^{2+}$ ions detection: A review. *J. Hazard. Mater.* **2022**, *424*, 127565. [CrossRef] [PubMed]
15. Su, M.; Liu, C.; Zhang, Y.; Rong, X.; Wang, X.; Li, X.; Wang, K.; Zhu, H.; Zhu, B. Rational design of a water-soluble TICT-AIEE-active fluorescent probe for mercury ion detection. *Anal. Chim. Acta* **2022**, *1230*, 340337. [CrossRef]
16. Yoon, S.; Miller, E.W.; He, Q.; Do, P.H.; Chang, C.J. A bright and specific fluorescent sensor for mercury in water, cells, and tissue. *Angew. Chem.* **2007**, *119*, 6778–6781. [CrossRef]
17. Ribeiro, D.S.M.; Castro, R.C.; Páscoa, R.N.M.J.; Soares, J.X.; Rodrigues, S.S.M.; Santos, J.L.M. Tuning CdTe quantum dots reactivity for multipoint detection of mercury (II), silver (I) and copper (II). *J. Lumin.* **2019**, *207*, 386–396. [CrossRef]

18. Labeb, M.; Sakr, A.-H.; Soliman, M.; Abdel-Fattah, T.M.; Ebrahim, S. Effect of capping agent on selectivity and sensitivity of CdTe quantum dots optical sensor for detection of mercury ions. *Opt. Mater.* **2018**, *79*, 331–335. [CrossRef]
19. Ke, J.; Li, X.; Zhao, Q.; Hou, Y.; Chen, J. Ultrasensitive quantum dot fluorescence quenching assay for selective detection of mercury ions in drinking water. *Sci. Rep.* **2014**, *4*, 5624. [CrossRef]
20. Bano, D.; Kumar, V.; Singh, V.K.; Hasan, S.H. Green synthesis of fluorescent carbon quantum dots for the detection of mercury (II) and glutathione. *New J. Chem.* **2018**, *42*, 5814–5821. [CrossRef]
21. Kou, X.; Jiang, S.; Park, S.-J.; Meng, L.-Y. A review: Recent advances in preparations and applications of heteroatom-doped carbon quantum dots. *Dalton Trans.* **2020**, *49*, 6915–6938. [CrossRef] [PubMed]
22. Azami, M.; Wei, J.; Valizadehderakhshan, M.; Jayapalan, A.; Ayodele, O.O.; Nowlin, K. Effect of Doping Heteroatoms on the Optical Behaviors and Radical Scavenging Properties of Carbon Nanodots. *J. Phys. Chem. C* **2023**, *127*, 7360–7370. [CrossRef]
23. Resch-Genger, U.; Grabolle, M.; Cavaliere-Jaricot, S.; Nitschke, R.; Nann, T. Quantum dots versus organic dyes as fluorescent labels. *Nat. Methods* **2008**, *5*, 763–775. [CrossRef] [PubMed]
24. Liu, T.; Li, N.; Dong, J.X.; Luo, H.Q.; Li, N.B. Fluorescence detection of mercury ions and cysteine based on magnesium and nitrogen co-doped carbon quantum dots and IMPLICATION logic gate operation. *Sens. Actuators B Chem.* **2016**, *231*, 147–153. [CrossRef]
25. Pajewska-Szmyt, M.; Buszewski, B.; Gadzała-Kopciuch, R. Sulphur and nitrogen doped carbon dots synthesis by microwave assisted method as quantitative analytical nano-tool for mercury ion sensing. *Mater. Chem. Phys.* **2020**, *242*, 122484. [CrossRef]
26. Tabish, T.A.; Hayat, H.; Abbas, A.; Narayan, R.J. Graphene Quantum Dots-Based Electrochemical Biosensing Platform for Early Detection of Acute Myocardial Infarction. *Biosensors* **2022**, *12*, 77. [CrossRef]
27. Javed, N.; O'Carroll, D.M. Carbon dots and stability of their optical properties. *Part. Part. Syst. Charact.* **2021**, *38*, 2000271. [CrossRef]
28. Wang, X.; Feng, Y.; Dong, P.; Huang, J. A mini review on carbon quantum dots: Preparation, properties, and electrocatalytic application. *Front. Chem.* **2019**, *7*, 671. [CrossRef]
29. Jagannathan, M.; Dhinasekaran, D.; Soundharraj, P.; Rajendran, S.; Vo, D.-V.N.; Prakasarao, A.; Ganesan, S. Green synthesis of white light emitting carbon quantum dots: Fabrication of white fluorescent film and optical sensor applications. *J. Hazard. Mater.* **2021**, *416*, 125091. [CrossRef]
30. Kim, S.; Hwang, S.W.; Kim, M.-K.; Shin, D.Y.; Shin, D.H.; Kim, C.O.; Yang, S.B.; Park, J.H.; Hwang, E.; Choi, S.-H. Anomalous behaviors of visible luminescence from graphene quantum dots: Interplay between size and shape. *ACS Nano* **2012**, *6*, 8203–8208. [CrossRef]
31. Ahirwar, S.; Mallick, S.; Bahadur, D. Electrochemical method to prepare graphene quantum dots and graphene oxide quantum dots. *ACS Omega* **2017**, *2*, 8343–8353. [CrossRef] [PubMed]
32. Kumar, P.; Dhand, C.; Dwivedi, N.; Singh, S.; Khan, R.; Verma, S.; Singh, A.; Gupta, M.K.; Kumar, S.; Kumar, R. Graphene quantum dots: A contemporary perspective on scope, opportunities, and sustainability. *Renew. Sustain. Energy Rev.* **2022**, *157*, 111993. [CrossRef]
33. Sheely, A.; Gifford, B.; Tretiak, S.; Bishop, A. Tunable Optical Features of Graphene Quantum Dots from Edge Functionalization. *J. Phys. Chem. C* **2021**, *125*, 9244–9252. [CrossRef]
34. Tang, S.; Chen, D.; Wang, C.; Yang, Y.; Li, X.; Li, T.; Zhang, X. Preparation of concentration dependent nitrogen sulfur Co-doped graphene quantum dots by UV irradiation and reversible optical switch of hydroxypropyl methyl cellulose. *Dye. Pigment.* **2022**, *198*, 110022. [CrossRef]
35. Alas, M.O.; Alkas, F.B.; Aktas Sukuroglu, A.; Genc Alturk, R.; Battal, D. Fluorescent carbon dots are the new quantum dots: An overview of their potential in emerging technologies and nanosafety. *J. Mater. Sci.* **2020**, *55*, 15074–15105. [CrossRef]
36. Vibhute, A.; Patil, T.; Gambhir, R.; Tiwari, A.P. Fluorescent carbon quantum dots: Synthesis methods, functionalization and biomedical applications. *Appl. Surf. Sci. Adv.* **2022**, *11*, 100311. [CrossRef]
37. Gulati, S.; Baul, A.; Amar, A.; Wadhwa, R.; Kumar, S.; Varma, R.S. Eco-Friendly and Sustainable Pathways to Photoluminescent Carbon Quantum Dots (CQDs). *Nanomaterials* **2023**, *13*, 554. [CrossRef]
38. Xu, A.; Wang, G.; Li, Y.; Dong, H.; Yang, S.; He, P.; Ding, G. Carbon-based quantum dots with solid-state photoluminescent: Mechanism, implementation, and application. *Small* **2020**, *16*, 2004621. [CrossRef]
39. Gaurav, A.; Jain, A.; Tripathi, S.K. Review on Fluorescent Carbon/Graphene Quantum Dots: Promising Material for Energy Storage and Next-Generation Light-Emitting Diodes. *Materials* **2022**, *15*, 7888. [CrossRef]
40. Magesh, V.; Sundramoorthy, A.K.; Ganapathy, D. Recent advances on synthesis and potential applications of carbon quantum dots. *Front. Mater.* **2022**, *9*, 906838. [CrossRef]
41. Zhu, S.; Meng, Q.; Wang, L.; Zhang, J.; Song, Y.; Jin, H.; Zhang, K.; Sun, H.; Wang, H.; Yang, B. Highly photoluminescent carbon dots for multicolor patterning, sensors, and bioimaging. *Angew. Chem. Int. Ed.* **2013**, *52*, 3953–3957. [CrossRef] [PubMed]
42. Jing, S.; Zhao, Y.; Sun, R.-C.; Zhong, L.; Peng, X. Facile and high-yield synthesis of carbon quantum dots from biomass-derived carbons at mild condition. *ACS Sustain. Chem. Eng.* **2019**, *7*, 7833–7843. [CrossRef]
43. Kalluri, A.; Debnath, D.; Dharmadhikari, B.; Patra, P. Chapter Twelve—Graphene Quantum Dots: Synthesis and Applications. In *Methods in Enzymology*; Kumar, C.V., Ed.; Academic Press: Cambridge, MA, USA, 2018; pp. 335–354.
44. Yuan, F.; Li, S.; Fan, Z.; Meng, X.; Fan, L.; Yang, S. Shining carbon dots: Synthesis and biomedical and optoelectronic applications. *Nano Today* **2016**, *11*, 565–586. [CrossRef]

45. Fernando, K.A.S.; Sahu, S.; Liu, Y.; Lewis, W.K.; Guliants, E.A.; Jafariyan, A.; Wang, P.; Bunker, C.E.; Sun, Y.-P. Carbon quantum dots and applications in photocatalytic energy conversion. *ACS Appl. Mater. Interfaces* **2015**, *7*, 8363–8376. [CrossRef] [PubMed]
46. Luo, Z.; Qi, G.; Chen, K.; Zou, M.; Yuwen, L.; Zhang, X.; Huang, W.; Wang, L. Microwave-assisted preparation of white fluorescent graphene quantum dots as a novel phosphor for enhanced white-light-emitting diodes. *Adv. Funct. Mater.* **2016**, *26*, 2739–2744. [CrossRef]
47. Zhuo, S.; Shao, M.; Lee, S.-T. Upconversion and downconversion fluorescent graphene quantum dots: Ultrasonic preparation and photocatalysis. *ACS Nano* **2012**, *6*, 1059–1064. [CrossRef]
48. Li, L.L.; Ji, J.; Fei, R.; Wang, C.Z.; Lu, Q.; Zhang, J.R.; Jiang, L.P.; Zhu, J.J. A facile microwave avenue to electrochemiluminescent two-color graphene quantum dots. *Adv. Funct. Mater.* **2012**, *22*, 2971–2979. [CrossRef]
49. Rajender, G.; Giri, P.K. Formation mechanism of graphene quantum dots and their edge state conversion probed by photoluminescence and Raman spectroscopy. *J. Mater. Chem. C* **2016**, *4*, 10852–10865. [CrossRef]
50. Peng, J.; Gao, W.; Gupta, B.K.; Liu, Z.; Romero-Aburto, R.; Ge, L.; Song, L.; Alemany, L.B.; Zhan, X.; Gao, G.; et al. Graphene Quantum Dots Derived from Carbon Fibers. *Nano Lett.* **2012**, *12*, 844–849. [CrossRef]
51. Dong, Y.; Chen, C.; Zheng, X.; Gao, L.; Cui, Z.; Yang, H.; Guo, C.; Chi, Y.; Li, C.M. One-step and high yield simultaneous preparation of single- and multi-layer graphene quantum dots from CX-72 carbon black. *J. Mater. Chem.* **2012**, *22*, 8764–8766. [CrossRef]
52. Jin, H.; Huang, H.; He, Y.; Feng, X.; Wang, S.; Dai, L.; Wang, J. Graphene Quantum Dots Supported by Graphene Nanoribbons with Ultrahigh Electrocatalytic Performance for Oxygen Reduction. *J. Am. Chem. Soc.* **2015**, *137*, 7588–7591. [CrossRef] [PubMed]
53. Abbas, A.; Tabish, T.A.; Bull, S.J.; Lim, T.M.; Phan, A.N. High yield synthesis of graphene quantum dots from biomass waste as a highly selective probe for $Fe^{3+}$ sensing. *Sci. Rep.* **2020**, *10*, 21262. [CrossRef] [PubMed]
54. Ghaffarkhah, A.; Hosseini, E.; Kamkar, M.; Sehat, A.A.; Dordanihaghighi, S.; Allahbakhsh, A.; van der Kuur, C.; Arjmand, M. Synthesis, applications, and prospects of graphene quantum dots: A comprehensive review. *Small* **2022**, *18*, 2102683. [CrossRef] [PubMed]
55. Somaraj, G.; Mathew, S.; Abraham, T.; Ambady, K.G.; Mohan, C.; Mathew, B. Nitrogen and Sulfur Co-Doped Carbon Quantum Dots for Sensing Applications: A Review. *ChemistrySelect* **2022**, *7*, e202200473. [CrossRef]
56. Liu, Y.; Jiang, L.; Li, B.; Fan, X.; Wang, W.; Liu, P.; Xu, S.; Luo, X. Nitrogen doped carbon dots: Mechanism investigation and their application for label free CA125 analysis. *J. Mater. Chem. B* **2019**, *7*, 3053–3058. [CrossRef]
57. Nguyen, K.G.; Baragau, I.-A.; Gromicova, R.; Nicolaev, A.; Thomson, S.A.J.; Rennie, A.; Power, N.P.; Sajjad, M.T.; Kellici, S. Investigating the effect of N-doping on carbon quantum dots structure, optical properties and metal ion screening. *Sci. Rep.* **2022**, *12*, 13806. [CrossRef]
58. Yang, S.; Sun, J.; Li, X.; Zhou, W.; Wang, Z.; He, P.; Ding, G.; Xie, X.; Kang, Z.; Jiang, M. Large-scale fabrication of heavy doped carbon quantum dots with tunable-photoluminescence and sensitive fluorescence detection. *J. Mater. Chem. A* **2014**, *2*, 8660–8667. [CrossRef]
59. Cheng, Z.; Du, F.; Sun, L.; Jiang, L.; Ruan, G.; Li, J. Nitrogen-Doped Carbon Quantum Dots as a "Turn-Off" Fluorescent Probes for Highly Selective and Sensitive Detection of Mercury (II) Ions. *ChemistrySelect* **2019**, *4*, 2122–2128. [CrossRef]
60. Luo, L.; Wang, P.; Wang, Y.; Wang, F. pH assisted selective detection of Hg (II) and Ag (I) based on nitrogen-rich carbon dots. *Sens. Actuators B Chem.* **2018**, *273*, 1640–1647. [CrossRef]
61. Guo, H.; Raj, J.; Wang, Z.; Zhang, T.; Wang, K.; Lin, L.; Hou, W.; Zhang, J.; Wu, M.; Wu, J. Synergistic Effects of Amine Functional Groups and Enriched-Atomic-Iron Sites in Carbon Dots for Industrial-Current–Density $CO_2$ Electroreduction. *Small* **2024**, *20*, 2311132. [CrossRef]
62. Gao, H.; Liu, Z.; Song, L.; Guo, W.; Gao, W.; Ci, L.; Rao, A.; Quan, W.; Vajtai, R.; Ajayan, P.M. Synthesis of S-doped graphene by liquid precursor. *Nanotechnology* **2012**, *23*, 275605. [CrossRef] [PubMed]
63. Ge, J.; Jia, Q.; Liu, W.; Guo, L.; Liu, Q.; Lan, M.; Zhang, H.; Meng, X.; Wang, P. Red-emissive carbon dots for fluorescent, photoacoustic, and thermal theranostics in living mice. *Adv. Mater.* **2015**, *27*, 4169–4177. [CrossRef]
64. Wu, F.; Yang, M.; Zhang, H.; Zhu, S.; Zhu, X.; Wang, K. Facile synthesis of sulfur-doped carbon quantum dots from vitamin B1 for highly selective detection of $Fe^{3+}$ ion. *Opt. Mater.* **2018**, *77*, 258–263. [CrossRef]
65. Li, S.; Li, Y.; Cao, J.; Zhu, J.; Fan, L.; Li, X. Sulfur-Doped Graphene Quantum Dots as a Novel Fluorescent Probe for Highly Selective and Sensitive Detection of $Fe^{3+}$. *Anal. Chem.* **2014**, *86*, 10201–10207. [CrossRef] [PubMed]
66. Park, C.H.; Yang, H.; Lee, J.; Cho, H.-H.; Kim, D.; Lee, D.C.; Kim, B.J. Multicolor Emitting Block Copolymer-Integrated Graphene Quantum Dots for Colorimetric, Simultaneous Sensing of Temperature, pH, and Metal Ions. *Chem. Mater.* **2015**, *27*, 5288–5294. [CrossRef]
67. Shen, X.; Wang, Z.; Guo, H.; Lei, Z.; Liu, Z.; Wang, L. Solvent engineering of oxygen-enriched carbon dots for efficient electrochemical hydrogen peroxide production. *Small* **2023**, *19*, 2303156. [CrossRef]
68. Hu, B.; Huang, K.; Tang, B.; Lei, Z.; Wang, Z.; Guo, H.; Lian, C.; Liu, Z.; Wang, L. Graphene quantum dot-mediated atom-layer semiconductor electrocatalyst for hydrogen evolution. *Nano-Micro Lett.* **2023**, *15*, 217. [CrossRef] [PubMed]
69. Yarur, F.; Macairan, J.-R.; Naccache, R. Ratiometric detection of heavy metal ions using fluorescent carbon dots. *Environ. Sci. Nano* **2019**, *6*, 1121–1130. [CrossRef]
70. Li, C.; Liu, W.; Ren, Y.; Sun, X.; Pan, W.; Wang, J. The selectivity of the carboxylate groups terminated carbon dots switched by buffer solutions for the detection of multi-metal ions. *Sens. Actuators B Chem.* **2017**, *240*, 941–948. [CrossRef]

71. Bhamore, J.R.; Park, T.J.; Kailasa, S.K. Glutathione-capped Syzygium cumini carbon dot-amalgamated agarose hydrogel film for naked-eye detection of heavy metal ions. *J. Anal. Sci. Technol.* **2020**, *11*, 13. [CrossRef]
72. Amjadi, M.; Jalili, R. A molecularly imprinted dual-emission carbon dot-quantum dot mesoporous hybrid for ratiometric determination of anti-inflammatory drug celecoxib. *Spectrochim. Acta Part A Mol. Biomol. Spectrosc.* **2018**, *191*, 345–351. [CrossRef]
73. Shahshahanipour, M.; Rezaei, B.; Ensafi, A.A.; Etemadifar, Z. An ancient plant for the synthesis of a novel carbon dot and its applications as an antibacterial agent and probe for sensing of an anti-cancer drug. *Mater. Sci. Eng. C* **2019**, *98*, 826–833. [CrossRef] [PubMed]
74. Campos, B.B.; Contreras-Cáceres, R.; Bandosz, T.J.; Jiménez-Jiménez, J.; Rodríguez-Castellón, E.; da Silva, J.C.E.; Algarra, M. Carbon dots as fluorescent sensor for detection of explosive nitrocompounds. *Carbon* **2016**, *106*, 171–178. [CrossRef]
75. Babar, D.G.; Garje, S.S. Nitrogen and phosphorus co-doped carbon dots for selective detection of nitro explosives. *ACS Omega* **2020**, *5*, 2710–2717. [CrossRef]
76. Li, J.; Du, B.; Li, Y.; Wang, Y.; Wu, D.; Wei, Q. A turn-on fluorescent sensor for highly sensitive mercury (II) detection based on a carbon dot-labeled oligodeoxyribonucleotide and $MnO_2$ nanosheets. *New J. Chem.* **2018**, *42*, 1228–1234. [CrossRef]
77. Mandal, P.; Sahoo, D.; Sarkar, P.; Chakraborty, K.; Das, S. Fluorescence turn-on and turn-off sensing of pesticides by carbon dot-based sensor. *New J. Chem.* **2019**, *43*, 12137–12151. [CrossRef]
78. Ashrafi Tafreshi, F.; Fatahi, Z.; Ghasemi, S.F.; Taherian, A.; Esfandiari, N. Ultrasensitive fluorescent detection of pesticides in real sample by using green carbon dots. *PLoS ONE* **2020**, *15*, e0230646. [CrossRef] [PubMed]
79. Moonrinta, S.; Kwon, B.; In, I.; Kladsomboon, S.; Sajomsang, W.; Paoprasert, P. Highly biocompatible yogurt-derived carbon dots as multipurpose sensors for detection of formic acid vapor and metal ions. *Opt. Mater.* **2018**, *81*, 93–101. [CrossRef]
80. Gu, J.; Hu, D.; Wang, W.; Zhang, Q.; Meng, Z.; Jia, X.; Xi, K. Carbon dot cluster as an efficient "off–on" fluorescent probe to detect Au (III) and glutathione. *Biosens. Bioelectron.* **2015**, *68*, 27–33. [CrossRef]
81. Maiti, S.; Das, K.; Das, P.K. Label-free fluorimetric detection of histone using quaternized carbon dot–DNA nanobiohybrid. *Chem. Commun.* **2013**, *49*, 8851–8853. [CrossRef]
82. Freire, R.; Le, N.D.; Jiang, Z.; Kim, C.S.; Rotello, V.M.; Fechine, P. $NH_2$-rich Carbon Quantum Dots: A protein-responsive probe for detection and identification. *Sens. Actuators B Chem.* **2018**, *255*, 2725–2732. [CrossRef]
83. Godavarthi, S.; Kumar, K.M.; Vélez, E.V.; Hernandez-Eligio, A.; Mahendhiran, M.; Hernandez-Como, N.; Aleman, L.; Gomez, L.M. Nitrogen doped carbon dots derived from Sargassum fluitans as fluorophore for DNA detection. *J. Photochem. Photobiol. B Biol.* **2017**, *172*, 36–41. [CrossRef] [PubMed]
84. Bhattacharya, S.; Nandi, S.; Jelinek, R. Carbon-dot–hydrogel for enzyme-mediated bacterial detection. *RSC Adv.* **2017**, *7*, 588–594. [CrossRef]
85. Ahmadian-Fard-Fini, S.; Ghanbari, D.; Salavati-Niasari, M. Photoluminescence carbon dot as a sensor for detecting of Pseudomonas aeruginosa bacteria: Hydrothermal synthesis of magnetic hollow $NiFe_2O_4$-carbon dots nanocomposite material. *Compos. Part B Eng.* **2019**, *161*, 564–577. [CrossRef]
86. Cao, J.; Zhang, H.; Nian, Q.; Xu, Q. Electrospun chitosan/polyethylene oxide nanofibers mat loaded with copper (II) as a new sensor for colorimetric detection of tetracycline. *Int. J. Biol. Macromol.* **2022**, *212*, 527–535. [CrossRef]
87. Msto, R.K.; Othman, H.O.; Al-Hashimi, B.R.; Salahuddin Ali, D.; Hassan, D.H.; Hassan, A.Q.; Smaoui, S. Fluorescence Turns on-off-on Sensing of Ferric Ion and L-Ascorbic Acid by Carbon Quantum Dots. *J. Food Qual.* **2023**, *2023*, 5555608. [CrossRef]
88. Han, Y.; Shi, L.; Luo, X.; Chen, X.; Yang, W.; Tang, W.; Wang, J.; Yue, T.; Li, Z. A signal-on fluorescent sensor for ultra-trace detection of $Hg^{2+}$ via $Ag^{+}$ mediated sulfhydryl functionalized carbon dots. *Carbon* **2019**, *149*, 355–363. [CrossRef]
89. Gan, Z.; Hu, X.; Huang, X.; Li, Z.; Zou, X.; Shi, J.; Zhang, W.; Li, Y.; Xu, Y. A dual-emission fluorescence sensor for ultrasensitive sensing mercury in milk based on carbon quantum dots modified with europium (III) complexes. *Sens. Actuators B Chem.* **2021**, *328*, 128997. [CrossRef]
90. Ahmadian-Fard-Fini, S.; Ghanbari, D.; Amiri, O.; Salavati-Niasari, M. Electro-spinning of cellulose acetate nanofibers/Fe/carbon dot as photoluminescence sensor for mercury (II) and lead (II) ions. *Carbohydr. Polym.* **2020**, *229*, 115428. [CrossRef]
91. Ghanem, A.; Al-Marjeh, R.A.-Q.B.; Atassi, Y. Novel nitrogen-doped carbon dots prepared under microwave-irradiation for highly sensitive detection of mercury ions. *Heliyon* **2020**, *6*, e03750. [CrossRef]
92. Muthurasu, A.; Ganesh, V. Tuning optical properties of nitrogen-doped carbon dots through fluorescence resonance energy transfer using Rhodamine B for the ratiometric sensing of mercury ions. *Anal. Methods* **2021**, *13*, 1857–1865. [CrossRef]
93. Yahyazadeh, E.; Shemirani, F. Easily synthesized carbon dots for determination of mercury (II) in water samples. *Heliyon* **2019**, *5*, e01596. [PubMed]
94. He, J.H.; Cheng, Y.Y.; Yang, T.; Zou, H.Y.; Huang, C.Z. Functional preserving carbon dots-based fluorescent probe for mercury (II) ions sensing in herbal medicines via coordination and electron transfer. *Anal. Acta* **2018**, *1035*, 203–210. [CrossRef] [PubMed]
95. Liao, S.; Zhang, L.; Li, S.; Yue, S.; Wang, G. Selective detection of mercury ions via single and dual signals by silicon-doped carbon quantum dots. *New J. Chem.* **2023**, *47*, 14242–14248. [CrossRef]
96. Chaghaghazardi, M.; Kashanian, S.; Nazari, M.; Omidfar, K.; Joseph, Y.; Rahimi, P. Nitrogen and sulfur co-doped carbon quantum dots fluorescence quenching assay for detection of mercury (II). *Spectrochim. Acta Part A Mol. Biomol. Spectrosc.* **2023**, *293*, 122448. [CrossRef]
97. Omer, K.M.; Aziz, K.H.H.; Mohammed, S.J. Improvement of selectivity via the surface modification of carbon nanodots towards the quantitative detection of mercury ions. *New J. Chem.* **2019**, *43*, 12979–12986. [CrossRef]

98. Lu, C.; Ding, H.; Wang, Y.; Xiong, C.; Wang, X. Colorimetric and turn-on fluorescence determination of mercury (II) by using carbon dots and gold nanoparticles. *Nanotechnology* **2021**, *32*, 155501. [CrossRef]
99. Li, B.; Ma, H.; Zhang, B.; Qian, J.; Cao, T.; Feng, H.; Li, W.; Dong, Y.; Qin, W. Dually emitting carbon dots as fluorescent probes for ratiometric fluorescent sensing of pH values, mercury (II), chloride and Cr (VI) via different mechanisms. *Microchim. Acta* **2019**, *186*, 341. [CrossRef]
100. Ren, H.; Labidi, A.; Sun, J.; Allam, A.A.; Ajarem, J.S.; Abukhadra, M.R.; Wang, C. Facile synthesis of nitrogen, sulfur co-doped carbon quantum dots for selective detection of mercury (II). *Environ. Chem. Lett.* **2024**, *22*, 35–41. [CrossRef]
101. Hao, X.; Dai, S.; Wang, J.; Fang, Z. Synthesis of blue fluorescent carbon dots and their application in detecting mercury and iodine based on "off–on" mode. *Luminescence* **2021**, *36*, 721–732. [CrossRef]
102. Wang, S.; Chen, H.; Xie, H.; Wei, L.; Xu, L.; Zhang, L.; Lan, W.; Zhou, C.; She, Y.; Fu, H. A novel thioctic acid-carbon dots fluorescence sensor for the detection of $Hg^{2+}$ and thiophanate methyl via S-Hg affinity. *Food Chem.* **2021**, *346*, 128923. [CrossRef] [PubMed]
103. Ge, L.; Hu, G.; Zhao, F.; Wang, X.; Ma, Z.; Liu, R. Carbon dots prepared by thermal reactions and selective detections of copper and mercury ions in visible spectrum. *Appl. Phys. A* **2021**, *127*, 388. [CrossRef]
104. Tang, W.; Wang, Y.; Wang, P.; Di, J.; Yang, J.; Wu, Y. Synthesis of strongly fluorescent carbon quantum dots modified with polyamidoamine and a triethoxysilane as quenchable fluorescent probes for mercury (II). *Microchim. Acta* **2016**, *183*, 2571–2578. [CrossRef]
105. Achadu, O.J.; Revaprasadu, N. Microwave-assisted synthesis of thymine-functionalized graphitic carbon nitride quantum dots as a fluorescent nanoprobe for mercury (II). *Microchim. Acta* **2018**, *185*, 461. [CrossRef] [PubMed]
106. Karami, C.; Taher, M.A.; Shahlaei, M. A simple method for determination of mercury (II) ions by PNBS-doped carbon dots as a fluorescent probe. *J. Mater. Sci. Mater. Electron.* **2020**, *31*, 5975–5983. [CrossRef]
107. Lan, M.; Zhang, J.; Chui, Y.-S.; Wang, P.; Chen, X.; Lee, C.-S.; Kwong, H.-L.; Zhang, W. Carbon nanoparticle-based ratiometric fluorescent sensor for detecting mercury ions in aqueous media and living cells. *ACS Appl. Mater. Interfaces* **2014**, *6*, 21270–21278. [CrossRef]
108. Aziz, K.H.H.; Omer, K.M.; Hamarawf, R.F. Lowering the detection limit towards nanomolar mercury ion detection via surface modification of N-doped carbon quantum dots. *New J. Chem.* **2019**, *43*, 8677–8683. [CrossRef]
109. Guo, H.; Wang, X.; Wu, N.; Xu, M.; Wang, M.; Zhang, L.; Yang, W. In-situ synthesis of carbon dots-embedded europium metal-organic frameworks for ratiometric fluorescence detection of $Hg^{2+}$ in aqueous environment. *Anal. Acta* **2021**, *1141*, 13–20. [CrossRef]
110. Xie, Y.; Cheng, D.; Liu, X.; Han, A. Green hydrothermal synthesis of N-doped carbon dots from biomass highland barley for the detection of $Hg^{2+}$. *Sensors* **2019**, *19*, 3169. [CrossRef]
111. Gómez Pineros, B.S.; Granados-Oliveros, G. L-cysteine modified N-doped carbon quantum dots derived from peach palm (Bactris gasipaes) peels for detection of mercury ions. *J. Mol. Struct.* **2024**, *1317*, 138990. [CrossRef]
112. Ananthanarayanan, A.; Wang, X.; Routh, P.; Sana, B.; Lim, S.; Kim, D.H.; Lim, K.H.; Li, J.; Chen, P. Facile synthesis of graphene quantum dots from 3D graphene and their application for $Fe^{3+}$ sensing. *Adv. Funct. Mater.* **2014**, *24*, 3021–3026. [CrossRef]
113. Gao, B.; Chen, D.; Gu, B.; Wang, T.; Wang, Z.; Yang, Y.; Guo, Q.; Wang, G. Facile and highly effective synthesis of nitrogen-doped graphene quantum dots as a fluorescent sensing probe for $Cu^{2+}$ detection. *Curr. Appl. Phys.* **2020**, *20*, 538–544. [CrossRef]
114. Kadian, S.; Sethi, S.K.; Manik, G. Recent advancements in synthesis and property control of graphene quantum dots for biomedical and optoelectronic applications. *Mater. Chem. Front.* **2021**, *5*, 627–658. [CrossRef]
115. Kongsanan, N.; Pimsin, N.; Keawprom, C.; Sricharoen, P.; Areerob, Y.; Nuengmatcha, P.; Oh, W.-C.; Chanthai, S.; Limchoowong, N. A fluorescence switching sensor for sensitive and selective detections of cyanide and ferricyanide using mercuric cation-graphene quantum dots. *ACS Omega* **2021**, *6*, 14379–14393. [CrossRef]
116. Li, J.; Wang, Z.; Yang, J.; Xia, X.; Yi, R.; Jiang, J.; Liu, W.; Chen, J.; Chen, L.; Xu, J. "On-off-on" fluorescence switch of graphene quantum dots: A cationic control strategy. *Appl. Surf. Sci.* **2021**, *546*, 149110. [CrossRef]
117. Gu, S.; Hsieh, C.-T.; Tsai, Y.-Y.; Ashraf Gandomi, Y.; Yeom, S.; Kihm, K.D.; Fu, C.-C.; Juang, R.-S. Sulfur and nitrogen co-doped graphene quantum dots as a fluorescent quenching probe for highly sensitive detection toward mercury Ions. *ACS Appl. Nano Mater.* **2019**, *2*, 790–798. [CrossRef]
118. Liu, Y.; Tang, X.; Deng, M.; Cao, Y.; Li, Y.; Zheng, H.; Li, F.; Yan, F.; Lan, T.; Shi, L. Nitrogen doped graphene quantum dots as a fluorescent probe for mercury (II) ions. *Microchim. Acta* **2019**, *186*, 140. [CrossRef]
119. Anh, N.T.N.; Chowdhury, A.D.; Doong, R.-A. Highly sensitive and selective detection of mercury ions using N, S-codoped graphene quantum dots and its paper strip based sensing application in wastewater. *Sens. Actuators B Chem.* **2017**, *252*, 1169–1178. [CrossRef]
120. Yang, Y.; Xiao, X.; Xing, X.; Wang, Z.; Zou, T.; Wang, Z.; Zhao, R.; Wang, Y. One-pot synthesis of N-doped graphene quantum dots as highly sensitive fluorescent sensor for detection of mercury ions water solutions. *Mater. Res. Express* **2019**, *6*, 095615. [CrossRef]
121. Zhu, Q.; Mao, H.; Li, J.; Hua, J.; Wang, J.; Yang, R.; Li, Z. A glycine-functionalized graphene quantum dots synthesized by a facile post-modification strategy for a sensitive and selective fluorescence sensor of mercury ions. *Spectrochim. Acta Part A Mol. Biomol. Spectrosc.* **2021**, *247*, 119090. [CrossRef]

122. Peng, D.; Zhang, L.; Liang, R.-P.; Qiu, J.-D. Rapid detection of mercury ions based on nitrogen-doped graphene quantum dots accelerating formation of manganese porphyrin. *ACS Sens.* **2018**, *3*, 1040–1047. [CrossRef]
123. Chini, M.K.; Kumar, V.; Javed, A.; Satapathi, S. Graphene quantum dots and carbon nano dots for the FRET based detection of heavy metal ions. *Nano-Struct. Nano-Objects* **2019**, *19*, 100347. [CrossRef]